Ultrasonic propagation through hydrating cements

C.M. Sayers and R.L. Grenfell

Schlumberger Cambridge Research, PO Box 153, Cambridge CB3 0HG, UK
Received 13 July 1992; revised 9 November 1992

Hydraulic cements develop mechanical strength and low permeability as a result of hydration, which involves chemical reactions between water and the anhydrous compounds present in the cement. Solid hydration products form both at the surfaces of the cement particles and in the pore space by nucleation and aggregation. As a result, the solid phase becomes highly connected and the material transforms from a viscous suspension of irregularly-shaped cement particles into a porous elastic solid with non-vanishing bulk and shear moduli. This transition to an interconnected solid phase is an example of a percolation transition. In this paper, measurements of the velocity of ultrasonic longitudinal and shear waves in ordinary Portland cement undergoing hydration are reported. The cement slurries were prepared in accordance with the American Petroleum Institute (API) specification for class G oil-well cement with various additives. After the time at which the cement becomes interconnected, the effective bulk and shear moduli are found to be linearly related and the effective Poisson's ratio is observed to decrease from the value of 0.5, characteristic of a fluid, to values characteristic of a porous elastic solid.

Keywords: cements; hydration; ultrasonic velocity; cement slurries

During oilfield drilling operations cement is placed in the annulus between the casing and formation in order to isolate different permeable zones. Formation fluids may enter the cemented annulus if the pressure exerted on a permeable zone falls below the formation pressure before the cement achieves sufficient mechanical strength and low enough permeability to prevent fluid invasion. Such invasion may lead to the loss of integrity of the cement sheath and, in the worst case, loss of the well.

Hydraulic cements develop mechanical strength and low permeability as a result of hydration, which involves chemical reactions between water and the anhydrous compounds present in the cement[1]. Solid hydration products form both at the surfaces of the cement particles and in the pore space by nucleation and aggregation. As a result, the solid phase becomes highly connected and the material transforms from a viscous suspension of irregularly-shaped cement particles into a porous elastic solid. This transition to an interconnected solid phase is an example of a percolation transition. The connectivity of the solid phase is responsible for the load-bearing capacity of set cement.

The velocity and attenuation of ultrasonic waves in inhomogeneous media can be used to characterize such media[2] and it is of interest to apply these techniques to study the time-evolving properties of cement. Keating *et al.*[3,4] have reviewed previous measurements of ultrasonic longitudinal pulse velocities in cement and have shown that after initial setting, the ultrasonic longitudinal pulse velocity is an effective method of differentiating between different slurries. As pointed out by Keating *et al.*[3,4], the water content is relatively high at early times so the initial longitudinal pulse velocity is governed by the fluid phase until the time at which the solid phase becomes interconnected. One purpose of this paper is to study this early-time behaviour in more detail.

In their review of previous work, Keating *et al.*[3,4] pointed out that some of the early-time measurements reported in the literature have been influenced by air trapped in the slurry due to the mixing procedure, and that the degree to which entrapped air influences results from pulse velocity measurements is currently disputed within the drilling industry. Rao *et al.*[5] described equipment capable of measuring ultrasonic velocities at a pressure of 140 MPa and thus capable of removing the problem of air bubbles. These authors have shown that the ultrasonic longitudinal wave velocity gives a good correlation with compressive strength for a range of oil-field slurries.

In recent work, D'Angelo *et al.*[6] examined the propagation of ultrasonic longitudinal and shear waves in cement slurries and showed that ultrasonic shear waves are more sensitive to the connectivity of the cement matrix than are longitudinal waves. These authors report a correlation between the onset of shear-wave propagation and measured API thickening times. Ultrasonic compression and shear waves have also been used to study the hydration of cements and mortars at longer times.[7,8]

In this paper, measurements of the velocity of ultrasonic longitudinal and shear waves in ordinary Portland cement undergoing hydration are reported. The apparatus used is similar to that of D'Angelo *et al.*[6] The

0041-624X/93/030147-07

measurements are analysed using the theory developed by Biot[9] of elastic wave propagation in a porous elastic solid saturated with a compressible viscous fluid. The cement slurries were prepared in accordance with the American Petroleum Institute (API) specification for class G oil-well cement with various additives. In order to minimize the effect of air bubbles, measurements were made on de-aerated and rolled slurries.

Theory

Ultrasonic propagation in suspensions

The theory for the velocity and attenuation of ultrasound in suspensions has recently been reviewed by Harker and Temple[10] and extended to polydisperse suspensions by Harker *et al.*[11] The effective wave velocity and attenuation of an ultrasonic wave of angular frequency ω in the suspension may be obtained from the real and imaginary parts of the complex wave-number k, describing wave propagation in the suspension. Harker *et al.*[11] showed that the results of Urick[12], Ament[13], Biot[9], Berryman,[14] Kuster and Toksoz[15], Schwartz and Plona[16] and Harker and Temple[10] for suspensions can all be written in the form:

$$k^2 = \omega^2 \bar{\beta} \rho_{\text{eff}}(\omega) \tag{1}$$

where $\bar{\beta}$ is the mean compressibility of the suspension and is given by:

$$\bar{\beta} = (1 - \phi_s)\beta_f + \phi_s \beta_s \tag{2}$$

Here β_f and β_s are the compressibilities of the fluid and solid. $\rho_{\text{eff}}(\omega)$ is an effective density which depends on the volume fraction, ϕ_s, of the solid and the densities of the solid, ρ_s, and fluid, ρ_f. Harker *et al.*[11] showed that $\rho_{\text{eff}}(\omega)$ may be written in the form:

$$\rho_{\text{eff}}(\omega) = \bar{\rho} - \frac{\phi_s(1 - \phi_s)\delta\rho^2}{M(\omega) + [\phi_s \rho_f + (1 - \phi_s)\rho_s]} \tag{3}$$

Here $\bar{\rho} = \phi_s \rho_s + (1 - \phi_s)\rho_f$ is the mean density and $\delta\rho = \rho_s - \rho_f$ is the density difference. Harker *et al.*[11] gave expressions for $M(\omega)$ derived for suspensions from the theories of Urick[12], Ament[13], Biot[9], Berrymann[14], Kuster and Toksoz[15], Schwartz and Plona[16] and Harker and Temple[10]. For example, the theory of Biot[9] gives

$$M(\omega) = \frac{\alpha - 1}{\phi_s}\rho_f \tag{4}$$

for suspensions, where $\alpha \geqslant 1$ is a purely geometrical quantity which is independent of the solid and fluid densities[17]. For the case of isolated spherical particles in a fluid, Berrymann[14] obtained the following equation for α:

$$\alpha = \frac{1(2 - \phi_s)}{2(1 - \phi_s)} \tag{5}$$

Cement as a porous elastic solid

As a result of hydration, cement begins to acquire mechanical strength as the material transforms from a viscous suspension of irregularly shaped cement particles into a porous elastic solid. It is therefore more appropriate to treat the material as a porous elastic solid with a porous 'frame' characterized by a bulk modulus K and shear modulus G. These frame moduli characterize the deformation of the material under 'drained' conditions which correspond to the fluid pressure being held constant during the deformation. The propagation of elastic waves in a porous elastic solid saturated with a compressible viscous fluid has been treated by Biot[9]. An important result is that there exist two longitudinal waves in a fluid-saturated permeable solid, a fast wave corresponding to the solid and fluid moving in phase, and a slow wave corresponding to the solid and fluid moving out of phase. If the pore fluid has viscosity η, the slow wave is diffusive at low frequencies, the critical frequency separating the low and high frequency regimes corresponding to the viscous skin depth, $(2\eta/\rho_f\omega)^{1/2}$, being of the same order as the pore size. At low frequencies, the skin depth is much greater than the pore size, so that fluid flow relative to the solid may be assumed to be of the Poiseuille type. As the frequency ω increases, the viscous skin depth, $(2\eta/\rho_f\omega)^{1/2}$, becomes small compared with the pore size and the high frequency form of Biot's theory becomes applicable.

Early-time behaviour. The centre frequency of the transducers used in the present work is about 0.5 MHz. At this frequency, the viscous skin depth in water is less than 1 μm compared with an initial pore size of order 30 μm for the cement slurries studied. At early times, therefore, the high frequency limit of Biot's theory should be used. In this limit, the three wave velocities are[17]:

$$v_s^2 = \frac{G}{(1 - \phi)\rho_s + (1 - \alpha^{-1})\phi\rho_f} \tag{6}$$

$$v_l^2(\text{fast, slow}) = \frac{\Delta \pm [\Delta^2 - 4(\rho_{11}\rho_{22} - \rho_{12}^2)(PR - Q^2)]^{1/2}}{2(\rho_{11}\rho_{22} - \rho_{12}^2)} \tag{7}$$

where α is the same geometrical parameter that appears in Equation (4) and ϕ is the porosity. In these equations[17]:

$$P = \frac{(1 - \phi)[1 - \phi - K/K_s]K_s + \phi K_s K/K_f}{1 - \phi - K/K_s + \phi K_s/K_f} + \frac{4}{3}G \tag{8}$$

$$Q = \frac{[1 - \phi - K/K_s]\phi K_s}{1 - \phi - K/K_s + \phi K_s/K_f} \tag{9}$$

$$R = \frac{\phi^2 K_s}{1 - \phi - K/K_s + \phi K_s/K_f} \tag{10}$$

and

$$\Delta = P\rho_{22} + R\rho_{11} - 2Q\rho_{12} \tag{11}$$

K_f and K_s are the bulk moduli of the fluid and solid. The density terms ρ_{ij} occurring in Equations (7) and (11) are related to the density of the solid, ρ_s, and fluid, ρ_f, by:

$$\rho_{11} + \rho_{12} = (1 - \phi)\rho_s \tag{12}$$

$$\rho_{22} + \rho_{12} = \phi\rho_f \tag{13}$$

$$\rho_{12} = -(\alpha - 1)\phi\rho_f \tag{14}$$

$(PR - Q^2)$ in Equation (7) may be written in the form:

$$(PR - Q^2) = \frac{(K + 4G/3)K_s\phi^2}{1 - \phi - K/K_s + \phi K_s/K_f} \tag{15}$$

In the limit of vanishing frame moduli, $K = G = 0$, the shear wave and slow longitudinal wave velocities vanish, as may be seen from Equations (6) and (7). The velocity

of the fast longitudinal wave in this limit agrees with that given by Equations (1)–(3) with $M(\omega)$ given by Equation (4). To first order in the frame moduli, the slow longitudinal wave velocity derived from Equation (7) agrees with that obtained by Johnson and Plona[17]:

$$v_1^2(\text{slow}) = \frac{(K + 4G/3)}{[(\phi - 2 + \alpha/\phi)\rho_f + (1 - \phi)\rho_s]} \quad (16)$$

The low velocity of the slow wave in the weak-frame limit implies that the wavelength of the slow wave is small compared with that of the fast wave and therefore that the attenuation due to scattering will be greater.

Longer-time behaviour. In contrast to the pore structure at early times, well-cured cements have little porosity with characteristic dimensions greater than 1 μm, the bulk of the porosity having dimensions less than 0.1 μm (see Reference 18). At longer times, therefore, the low frequency limit of Biot's theory is more appropriate[9]. In this limit the slow wave is diffusive whilst the shear wave velocity and fast longitudinal wave velocity are given by[9]:

$$v_s^2 = \frac{G}{(1 - \phi)\rho_s + \phi\rho_f} \quad (17)$$

$$v_1^2(\text{fast}) = \frac{H}{(1 - \phi)\rho_s + \phi\rho_f} \quad (18)$$

where $H = P + R + 2Q$. It follows from Equations (8)–(10) that:

$$H = (K + 4G/3) + \frac{K_f(K_s - K)^2}{K_f(K_s - K) + K_s(K_s - K_f)\phi} \quad (19)$$

If the cement particles are much less compressible than both the frame and pore fluid ($K_s \gg K_f$, K and G), Equation (19) reduces to:

$$H = (K + 4G/3) + \frac{K_f}{\phi} \quad (20)$$

In this regard, it should be noted that a small amount of entrapped air can reduce K_f considerably.

Experiment

Slurry preparation

The cement slurries were prepared in accordance with the American Petroleum Institute (API) specification for class G oil-well cement with the addition of various additives. Four types of slurry were studied:

(i) Neat slurry: 792 g cement, 349 g water.
(ii) Accelerated slurry: 792 g cement, 349 g water, 15.84 g $CaCl_2$ (2% by weight of cement).
(iii) Latex slurry.
(iv) Surfactant slurry.

Class G cements are intended for use from the surface to 2440 m (8000 ft) depth and contain 44% water by weight of cement. The addition of the $CaCl_2$ accelerator is appropriate for shallow wells. Latex slurries are made by adding an aqueous dispersion of solid polymer particles containing surfactants and protective colloids which impart stability to the dispersion. Slurries containing surfactants are designed to entrain invading gas downhole to create a stable foam[19]. For neat, accelerated and Latex slurries the preparation procedure was as follows. The required amounts of water and additives were placed in a 1 litre capacity Waring blender. The blender was run at 4000 rpm and the cement was then added in about 15 seconds. The cover of the blender was then replaced and the slurry was blended at 12000 rpm for 35 seconds. The slurries were then de-aerated by pouring the mixed slurry from the blender into an open-topped 1 litre beaker which was then put into a dessicator attached to a vacuum pump. The pump maintains a pressure of around 0.7 bar below atmospheric pressure for 20 minutes. The slurry was gently swirled every few minutes while under reduced pressure.

Surfactant slurries were prepared by mixing the slurry in the blender as described above but without the additives. The slurry was then placed together with the required additives in a 12 cm diameter 2 litre bottle which was then placed on a rolling machine such that the bottle revolved at about 0.27 rev s^{-1} for 20 minutes.

The ultrasonic test set-up

In this work the pulse transmission method was used. The experimental test set-up was similar to that described by D'Angelo *et al.*[6] and is shown schematically in *Figure 1*. After preparation, the cement slurry was poured into the perspex cell illustrated in the figure. This has internal dimensions 14 cm × 12 cm × 1.208 cm. The walls of the cell are 2.416 cm thick in order to separate the first arrival from multiple reflections in the cell walls.

The temperature of the slurry was monitored by placing a thermocouple in the sample. Ultrasonic velocity measurements were made using broad-band longitudinal

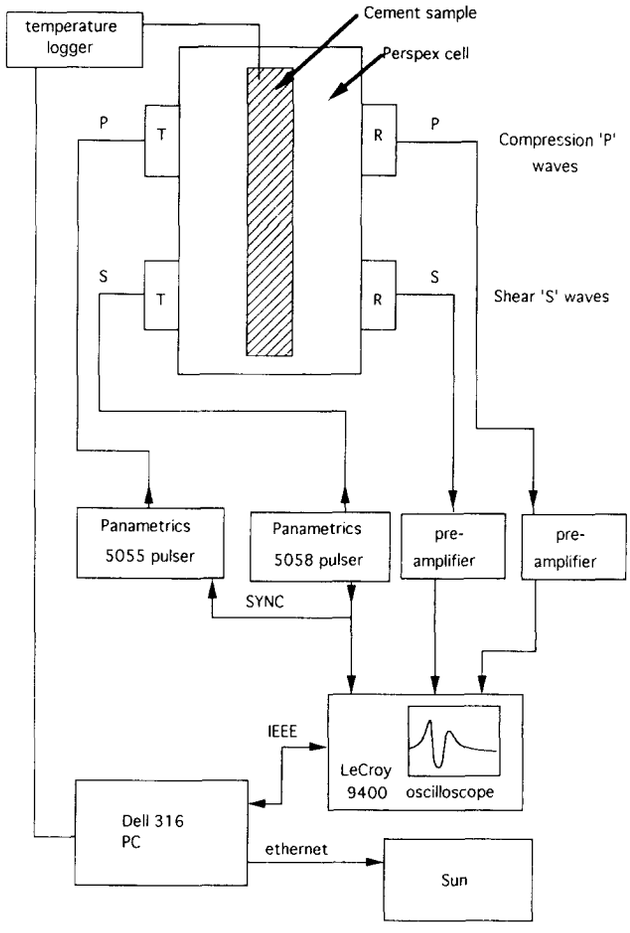

Figure 1 The ultrasonic experimental test set-up

(Panametrics V101-RB) and shear (Panametrics V151-RB) transducers with a nominal centre frequency of 0.5 MHz. A Panametrics 5055PR pulser/receiver was used to apply a pulse to the longitudinal wave transmitter whilst a Panametrics 5058PR high-voltage pulser/receiver was used to pulse the shear wave transmitter. A pulse repetition rate of 100 Hz was used. The ultrasonic pulse travels through the sample and is sensed by a second transducer, directly opposite the emitting transducer. Acoustic contact between the transducers and the outer walls of the cell was made with Panametrics couplant. The resulting electrical pulse is amplified by a Panametrics 5560B preamplifier. The amplified signal provides the input for a LeCroy 9400 digital oscilloscope.

Data were acquired at a 100 MHz sampling rate. Signal averaging was carried out by the oscilloscope using a fast averaging routine that takes about 10 s for 100 averages for the 20 000 time channels and the sampling rates used in this application. The data from the oscilloscope were transferred to a Dell 386SX IBM compatible PC during the test and later to a SUN workstation for further analysis. Averaged waveforms were acquired every five minutes.

Determination of the ultrasonic velocity

Wave velocities were determined by measuring the time taken for an ultrasonic pulse to traverse the sample. A suitable vertical amplification and sampling rate was selected on the oscilloscope so that the pulse fell within the digitization window. The sampling period used in the experiments was 10 ns. The time taken for the pulse to travel from the transmitter, through the cell walls and cement slurry to the receiver was determined from the waveform. This time was corrected for the time taken to travel through the walls, which was measured before the test. The corrected time delay and measured path length were then used to calculate the ultrasonic velocity in the slurry.

Results

The measured ultrasonic longitudinal wave velocities determined for these slurries are plotted in *Figures 2* and *3*. At early times a single longitudinal wave was observed with no evidence for a slow longitudinal wave or a shear wave. At later times, the solid frame became interconnected and a shear wave was observed. The measured shear wave velocities are plotted in *Figures 4* and *5*. No evidence for a slow longitudinal wave was found at later times. This is possibly the result of the pore size becoming comparable with the viscous skin depth at later times, the slow wave becoming diffusive.

The ultrasonic shear modulus G, calculated from Equation (17) using the shear-wave velocities plotted in *Figures 4* and *5*, and a calculated density for Class G cements of 1.9 g cm^{-3} is shown in *Figures 6* and *7*. *Figures 8* and *9* show plots of the longitudinal modulus

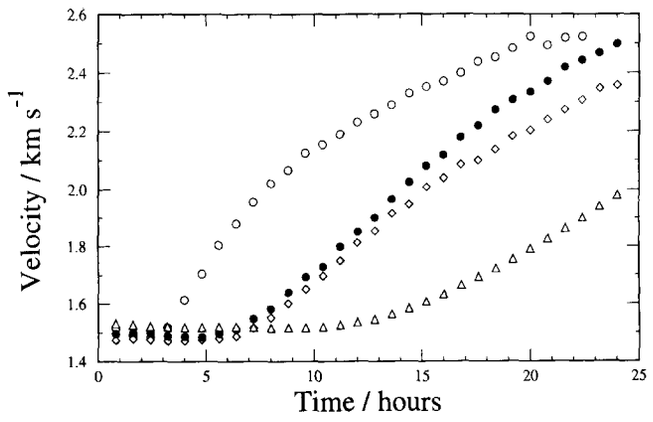

Figure 2 Measured ultrasonic longitudinal wave velocities for de-aerated and rolled Dykerhoff slurries: Dykerhoff + 2% $CaCl_2$ (○), neat Dykerhoff (●), surfactant Dykerhoff (◇) and Latex Dykerhoff (△)

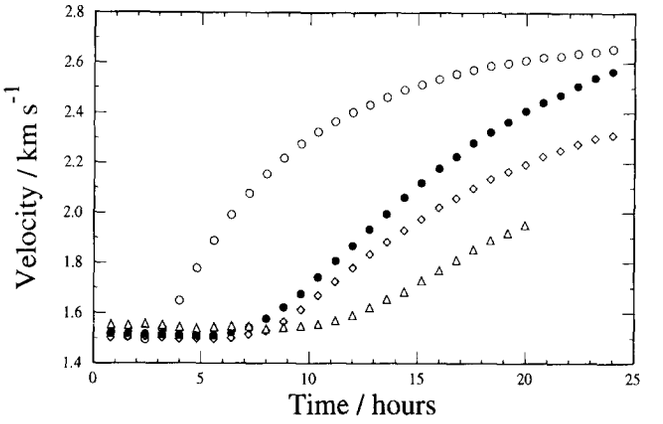

Figure 3 Measured ultrasonic longitudinal wave velocities for de-aerated and rolled Cemoil slurries: Cemoil + 2% $CaCl_2$ (○), neat Cemoil (●), surfactant Cemoil (◇) and Latex Cemoil (△)

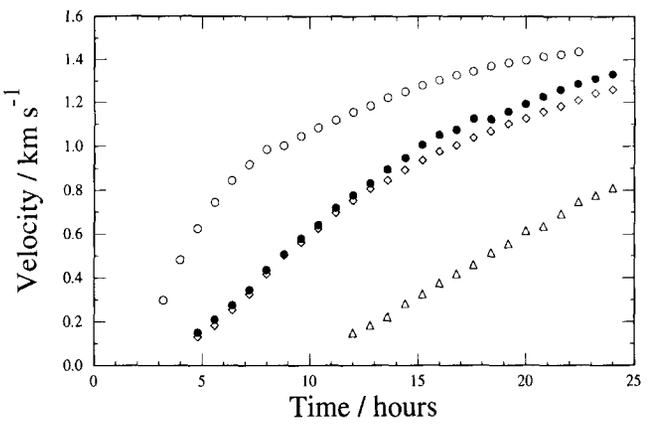

Figure 4 Measured ultrasonic shear wave velocities for de-aerated and rolled Dykerhoff slurries: Dykerhoff + 2% $CaCl_2$ (○), neat Dykerhoff (●), surfactant Dykerhoff (◇) and Latex Dykerhoff (△)

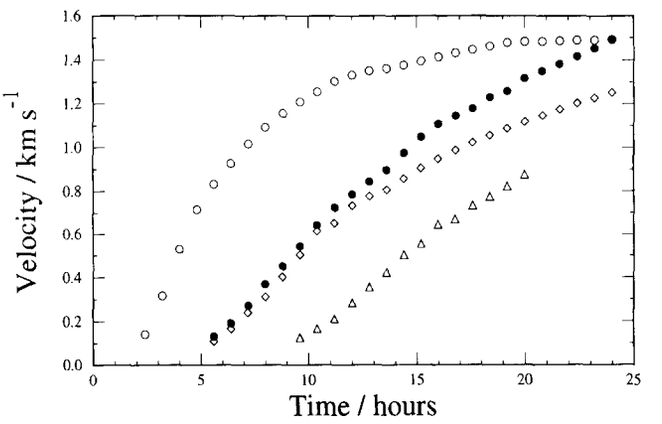

Figure 5 Measured ultrasonic shear wave velocities for de-aerated and rolled Cemoil slurries: Cemoil + 2% $CaCl_2$ (○), neat Cemoil (●), surfactant Cemoil (◇) and Latex Cemoil (△)

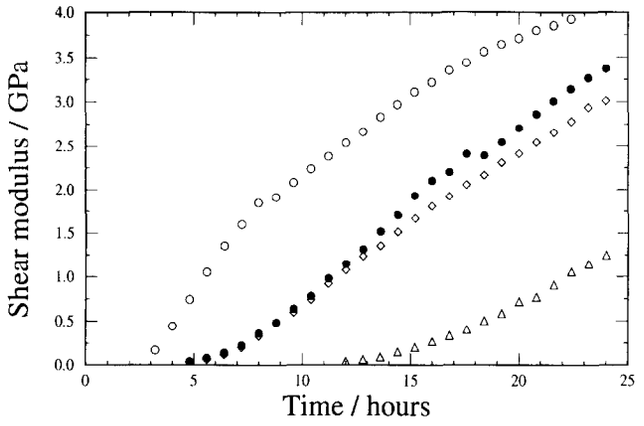

Figure 6 Ultrasonic shear modulus G for de-aerated and rolled Dykerhoff slurries: Dykerhoff + 2% $CaCl_2$ (○), neat Dykerhoff (●), surfactant Dykerhoff (◇) and Latex Dykerhoff (△)

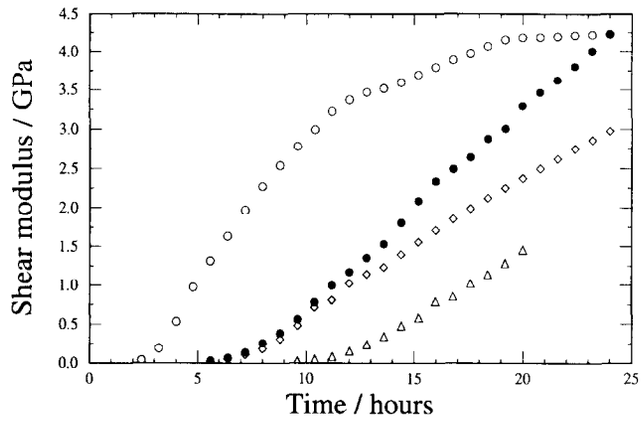

Figure 7 Ultrasonic shear modulus G for de-aerated and rolled Cemoil slurries: Cemoil + 2% $CaCl_2$ (○), neat Cemoil (●), surfactant Cemoil (◇) and Latex Cemoil (△)

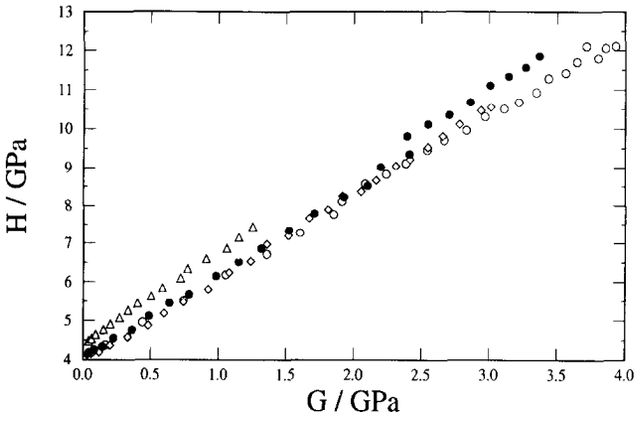

Figure 8 Ultrasonic longitudinal wave modulus H as a function of ultrasonic shear modulus G for de-aerated and rolled Dykerhoff slurries: Dykerhoff + 2% $CaCl_2$ (○), neat Dykerhoff (●), surfactant Dykerhoff (◇) and Latex Dykerhoff (△)

H, obtained from Equation (18) and the longitudinal-wave velocities plotted in *Figures 2* and *3*, against G. Comparing this with Equation (20) demonstrates that K_f/ϕ is similar for all of these slurries with the exception of the latex slurry, which appears to have a lower porosity. This is to be expected since the latex particles in the present formulation replace an equal volume of water, the particles having approximately the same density as water. It is apparent from *Figures 8* and *9* that after the

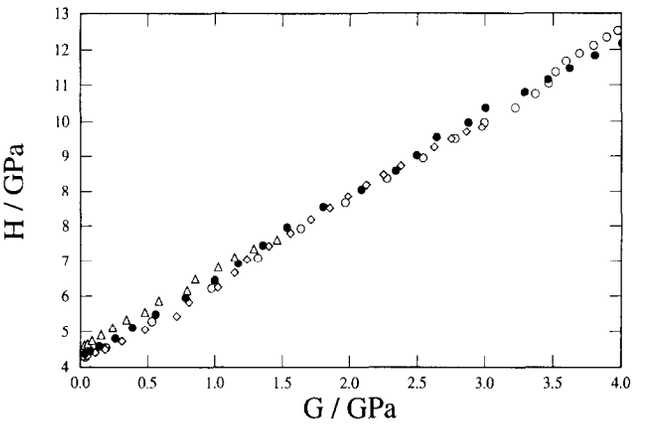

Figure 9 Ultrasonic longitudinal wave modulus H as a function of ultrasonic shear modulus G for de-aerated and rolled Cemoil slurries: Cemoil + 2% $CaCl_2$ (○), neat Cemoil (●), surfactant Cemoil (◇) and Latex Cemoil (△)

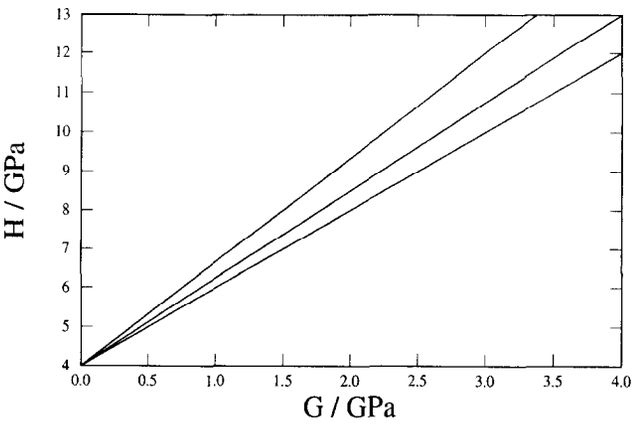

Figure 10 Ultrasonic longitudinal wave modulus H as a function of ultrasonic shear modulus G predicted from Equation (20) using a value $K_f/\phi = 4$ GPa deduced from the intercept in *Figures 8* and *9* for the cases $\nu = 0$ (bottom), $\nu = 0.1$ (middle) and $\nu = 0.2$ (top)

time at which the cement becomes interconnected, the effective bulk modulus is linearly related to the shear modulus.

If p is the volume fraction of solid and p_c is the value of p at which an interconnected solid phase first appears (the percolation threshold), the bulk modulus K and shear modulus G of the interconnected solid phase are expected to increase with increasing $p - p_c$ above the percolation threshold with the same critical exponent τ (see Reference 20):

$$K, G \propto (p - p_c)^{\tau} \tag{21}$$

In the neighbourhood of the percolation threshold the Poisson's ratio of the porous frame ν is therefore expected to be a constant. *Figure 10* shows the variation of H with G for constant ν predicted from Equation (20) assuming a constant value of $K_f/\phi = 4$ GPa deduced from the intercept in *Figures 8* and *9*. The curves plotted correspond to the cases $\nu = 0$, $\nu = 0.1$ and $\nu = 0.2$.

Figures 11 and *12* show the variation of the effective Poisson's ratio ν_{eff} with G. In terms of H and G, ν_{eff} is given by:

$$\nu_{eff} = \frac{(1 - 2G/H)}{2(1 - G/H)} \tag{22}$$

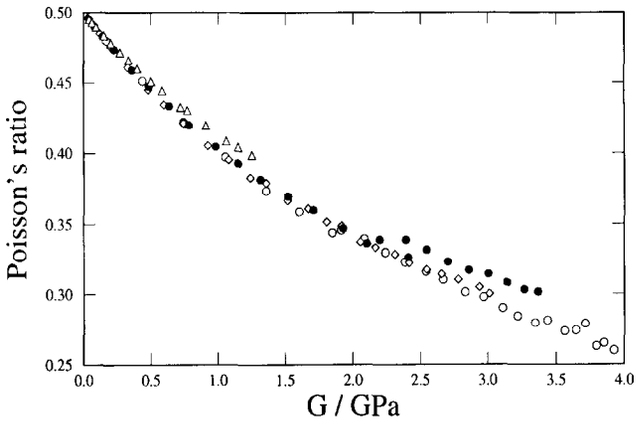

Figure 11 Effective Poisson's ratio ν_{eff} as a function of ultrasonic shear modulus G for de-aerated and rolled Dykerhoff slurries: Dykerhoff + 2%, $CaCl_2$ (○), neat Dykerhoff (●), surfactant Dykerhoff (◇) and Latex Dykerhoff (△)

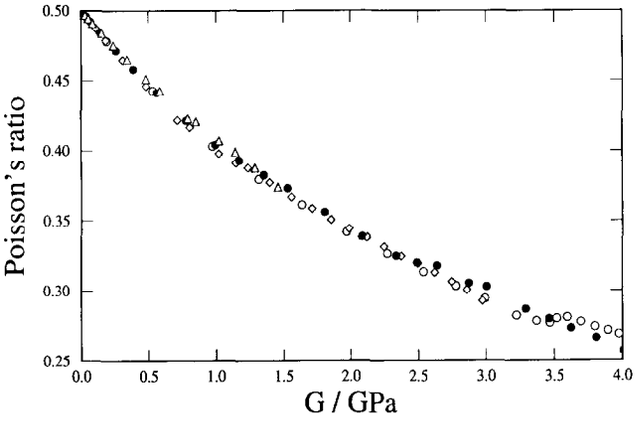

Figure 12 Effective Poisson's ratio ν_{eff} as a function of ultrasonic shear modulus G for de-aerated and rolled Cemoil slurries: Cemoil + 2% $CaCl_2$ (○), neat Cemoil (●), surfactant Cemoil (◇) and Latex Cemoil (△)

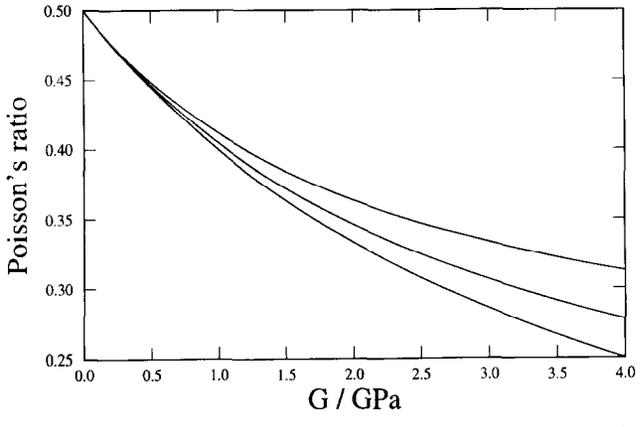

Figure 13 Effective Poisson's ratio ν_{eff} as a function of ultrasonic shear modulus G predicted from Equation (20) using a value $K_f/\phi = 4$ GPa deduced from the intercept in *Figures 8* and *9* for the cases $\nu = 0$ (bottom), $\nu = 0.1$ (middle) and $\nu = 0.2$ (top)

ν_{eff} lies in the range $1/2 \geqslant \nu_{eff} \geqslant \nu$, where ν is the Poisson's ratio of the porous frame. As time increases the solid phase becomes interconnected and the effective Poisson's ratio is observed to decrease from the value of 0.5, which is characteristic of a fluid.

Figure 13 shows the variation of ν_{eff} for constant ν predicted from Equation (20) assuming a constant value of $K_f/\phi = 4$ GPa deduced from the intercept in *Figures 8* and *9*. The curves plotted correspond to the cases $\nu = 0$, $\nu = 0.1$ and $\nu = 0.2$.

It follows from *Figures 8–13* that the assumption of a constant value of K_f/ϕ leads to a small calculated Poisson's ratio ν of the porous frame. It should be noted, however, that K_f/ϕ will vary during hydration. Cement total porosity ϕ decreases during the hydration process but at the same time chemical shrinkage generates new pores which increase the total porosity at the time of cement setting[18]. If, as a result of water being consumed during the reaction, the material becomes partially saturated, K_f will be substantially reduced and the Poisson's ratio plotted in *Figures 11* and *12* will correspond to that of the porous frame, as may be seen from Equation (20).

Conclusions

Measurements of the velocity of ultrasonic longitudinal and shear waves in ordinary Portland cement undergoing hydration have been presented. The cement slurries were prepared in accordance with the American Petroleum Institute (API) specification for class G oil-well cement with various additives. After the time at which the cement becomes interconnected, the effective bulk modulus of the cement is found to be linearly related to the effective shear modulus and the effective Poisson's ratio is observed to decrease from the value of 0.5 which is characteristic of a fluid, to values characteristic of a porous solid[21]. These results have important implications for the time evolution of the stress state within cemented annuli.

References

1 **Michaux, M., Nelson, E.B. and Vidick, B.** Chemistry and characterization of Portland cement. In *Well Cementing* (Ed. Nelson, E.B.) Schlumberger Educational Services, Houston (1990) 2-1–2-17

2 **Sayers, C.M.** Characterisation of microstructures using ultrasonics. In *Ultrasonic Methods in Evaluation of Inhomogeneous Materials* (Eds Alippi, A. and Mayer, W.G.) Martinus Nijhoff (1987) 175–183

3 **Keating, J., Hannant, D.J. and Hibbert, A.P.** Comparison of shear modulus and pulse velocity techniques to measure the build-up of structure in fresh cement pastes used in oilwell cementing *Cement and Concrete Res* (1980) **19** 554–566

4 **Keating, J., Hannant, D.H. and Hibbert, A.P.** Correlation between cube strength, ultrasonic pulse velocity and volume change for oilwell cement slurries *Cement and Concrete Res* (1989) **19** 715–726

5 **Rao, P.P., Sutton, D.L., Childs, J.D. and Cunningham, W.C.** An ultrasonic device for nondestructive testing of oil well cements at elevated temperatures and pressures *J Petroleum Technol* (1980) 2611–2616

6 **D'Angelo, R., Plona, T.J., Schwartz, L.M. and Coveney, P.** Ultrasonic measurements on hydrating cement slurries: the onset of shear-wave propagation. Paper submitted for publication in SPE Production Engineering (1992)

7 **Zimmerman, R.W., King, M.S. and Monteiro, P.J.M.** The elastic moduli of mortar as a porous-granular material *Cement and Concrete Res* **16** 239–245

8 **Monteiro, P.J.M. and King, M.S.** Experimental studies of elastic wave propagation in high-strength mortar *Cement, Concrete and Aggregates, CCAGDP* (1988) **10** 68–74

9 **Biot, M.A.** Theory of propagation of elastic waves in a fluid-saturated porous solid *J Acoust Am* **28** 168–191

10 **Harker, A.H. and Temple, J.A.G.** Velocity and attenuation of ultrasound in suspensions of particles in fluids *J Phys D: Appl Phys* (1988) **21** 1576–1588

11 **Harker, A.H., Schofield, P., Stimpson, B.P., Taylor, R.G. and Temple, J.A.G.** Ultrasonic propagation in slurries *Ultrasonics* (1988) **29** 427–438

12 **Urick, R.J.** A sound velocity method for determining the compressibility of finely divided substances *J Appl Phys* (1947) **18** 983–987

13 **Ament, W.S.** Sound propagation in gross mixtures *J Acoust Am* (1953) **25** 638–641

14 **Berrymann, J.G.** *Appl Phys Lett* (1980) **37** 382

15 **Kuster, G.T. and Toksoz, M.N.** *Geophys* (1974) **39** 587

16 **Schwartz, L. and Plona, T.J.** Ultrasonic propagation in close-packed disordered suspensions *J Appl Phys* (1985) **55** 3971–3977

17 **Johnson, D.L. and Plona, T.J.** Acoustic slow waves and the consolidation transition *J Acoust Soc Am* (1982) **72** 556–565

18 **Parcevaux, P.** Pore size distribution of portland cement slurries at very early stages of hydration *Cement and Concrete Res* (1984) **14** 419–430

19 **Parcevaux, P., Rae, P. and Drecq, P.** Prevention of annular gas migration. In *Well Cementing* (Ed Nelson, E.B.) Schlumberger Educational Services, Houston (1990) 8-1–8-22

20 **Bergman, D.J. and Kantor, Y.** Critical properties of an elastic fractal *Phys Rev Lett* (1984) **53** 511–514

21 **Sayers, C.M. and Smith, R.L.** The propagation of ultrasound in porous media *Ultrasonics* (1982) **20** 201–205